ISSN 2616-5880 Vol. 6, Issue 1: 59-65, DOI: 10.25236/AJMC.2025.060107

Constructing Robust and Efficient Ionic Conductive Interfaces for Utilizing SiO_x Anodes in Advanced Lithium-Ion Batteries with High Energy Density

Zenan Zhou[1,a], Dongliang Yan[1,b,*]

[1]School of Materials and Environment, Guangxi Minzhu University, Nanning, Guangxi, China
[a] 484009692@qq.com, [b]chemydl@163.com
**Corresponding author*

Abstract: *Silicon monoxide (SiO_x) material is considered a promising contender for anodes in high-power lithium-ion batteries owing to its high specific capacity. Nevertheless, the substantial volume fluctuation during the lithiation/delithiation cycles of SiO_x anodes leads to reduced initial coulombic efficiency (ICE) and capacity retention, hindering its practical implementation. To tackle this challenge, researchers have pre-fabricated a sturdy ionic conductive interface abundant in LiF, $Li_2C_2O_4$, $LiBO_2$, and $Li_2B_4O_7$ via a calcination process. This interface layer, distinguished by its high Young's modulus and swift Li^+ conductivity, can efficiently accommodate the plastic deformation of SiO_x anodes, curtail parasitic reactions, and preserve electrode integrity. The enhanced SiO_x (M-SiOx500°C) anode demonstrates improved ICE, superior capacity retention, and outstanding rate capability. A complete cell paired with a $LiNi_{0.8}Mn_{0.1}Co_{0.1}O_2$ cathode maintains a capacity level of 89.7% after 200 cycles. This study highlights the importance of pre-fabricating artificial solid-electrolyte interphase (SEI) layers and modifying interfacial chemistry to enhance the performance of SiO_x-based anodes, representing a notable step forward in the broad adoption of SiO_x-based anodes.*

Keywords: *Lithium difluorobis(oxalato)borate; Silicon suboxide; Lithium-ion Batteries; Interface engineering*

1. Introduction

Rechargeable lithium-ion batteries (LIBs) have become the favored power source for portable electronic devices, electric vehicles (EVs), and energy storage systems, due to their outstanding energy density, extended service life, and eco-friendliness[1-5]. In recent years, given the pressing need to increase the driving range of EVs, the advancement of LIBs featuring higher energy densities has become especially important[6-9]. One of the core strategies to achieve this goal is the adoption of novel anode materials with theoretical specific capacities far exceeding that of traditional graphite anodes (372 $mAhg^{-1}$), such as silicon monoxide (SiO_x, with a theoretical specific capacity ranging from 2200-2500 $mAhg^{-1}$) and silicon (Si, with a theoretical specific capacity up to 3800-4200 $mAhg^{-1}$).However, pure SiO_x and Si anodes experience significant volume expansions exceeding 200% and 300% during lithiation, respectively, resulting in severe electrode/particle cracking, damage to the solid electrolyte interphase (SEI) layer, and depletion of active lithium[10].In contrast, pure SiO_x shows higher promise because of its reduced volume expansion and enhanced cycling stability, thanks to the in-situ generated cushioning matrix composed of Li_2O and Li_xSiO_y, which efficiently absorbs the volume changes of SiO_x and promotes the formation of a stable SEI layer[11-12].Unfortunately, the inadequate electronic conductivity and the extra usage of active lithium linked to this buffering mechanism lead to subpar rate capability and a low initial charge-discharge efficiency (ICE), consequently impeding the straightforward application of pure SiO_x anodes in LIBs (full-cell setups) [13-14].

To tackle the issues encountered with SiO_x-based anodes, numerous approaches have been investigated, such as material alteration, electrolyte enhancement, and binder innovation[14-16].In terms of material alteration, surface coatings, elemental doping, and prelithiation methods are commonly utilized. For example, carbon coatings not only improve conductivity but also efficiently accommodate the volumetric changes of SiO_x-based anodes[15].To further promote the application of SiO_x anodes in LIBs, it is particularly necessary to improve the ICE of SiO_x anodes through thermally driven solid-phase reactions combined with prelithiation agents (such as lithium, lithium hydride).Although lithium fluoride (LiF) is well-known for its exceptional mechanical strength, elasticity, and chemical stability, the

ISSN 2616-5880 Vol. 6, Issue 1: 59-65, DOI: 10.25236/AJMC.2025.060107

formation of LiF in situ during the battery's charge-discharge cycles results in the depletion of active lithium. Therefore, preconstructing a dense and uniform artificial protective layer containing LiF during the synthesis stage of SiO_x anode materials has emerged as a promising strategy.

In this study, we innovatively preconstructed a robust and fast Li^+-conducting interlayer rich in LiF, $Li_2C_2O_4$, $LiBO_2$, and $Li_2B_4O_7$ on the surface of SiOx particles (modified SiO_x, M-SiO_x) by pyrolyzing lithium difluoro(oxalate)borate (LiDFOB). Although lithium fluoride (LiF) is well-known for its exceptional mechanical strength, elasticity, and chemical stability, the formation of LiF in situ during the battery's charge-discharge cycles results in the depletion of active lithium.Consequently, the M-SiO_x anode exhibits a higher ICE, superior capacity retention, and outstanding rate performance. Notably, a full-cell pairing the M-SiOx anode with a $LiNi_{0.8}Mn_{0.1}Co_{0.1}O_2$ cathode maintains a high capacity retention after 200 cycles. This study emphasizes the significance of preconstructing an artificial SEI layer and adjusting interfacial chemistry during material synthesis to improve the performance of SiO_x-based anodes.

2. Experimental section

2.1 Material preparation

Materials used: Materials used: Lithium difluoro(oxalato)borate (LiDFOB) and silicon monoxide SiO_x were purchased from Sinopharm Chemical Reagent Co., Ltd. and Guangdong Candlelight New Energy Technology Co., Ltd., respectively.

Commercial SiO_x and LiDFOB powders were mixed in a mass ratio of 20:1 and ground in a high-speed ball mill at a speed of 300 r/min for 4h to obtain the SiO_x/LiDFOB precursor. The obtained SiOx/LiDFOB was subsequently annealed at 500 °C for 2 hours in a pure argon environment, utilizing a heating rate of 5 °C/min.Upon cooling the mixture to room temperature, modified SiO_x (M-SiO_x) decorated with robust, fast ion-conducting interlayers was obtained. Another series of modified SiO_x was prepared using the same synthesis method.

2.2 Characterizations

The morphology, microstructure, and chemical composition of the prepared samples were investigated using a scanning electron microscope (SEM, Hitachi S4800) equipped with an energy-dispersive X-ray spectroscopy (EDS) detector. X-ray diffraction (XRD, Rigaku SmartLab) was employed to analyze the crystal phase and crystallinity of SiO_x and M-SiO_x. Additionally, X-ray photoelectron spectroscopy (XPS, Escalab 250XI) was utilized to determine the elemental composition and valence states of the materials.

2.3 Electrochemical measurements

To prepare the working electrodes, the active material, conductive carbon black (Super P), and sodium carboxymethyl cellulose (CMC) were mixed in a mass ratio of 8:1:1 in deionized water. The resulting slurry was uniformly coated onto copper foil using a doctor blade and then dried in a forced-air oven at 80°C for 12 hours. The copper foil was then cut into circular discs (Φ=14 mm) and further dried overnight under vacuum at 80°C to obtain the working electrodes. The mass loading of the anode was 1.3 mg cm^{-2}. Lithium metal foil and Celgard 2500 microporous membrane were used as the counter electrode and separator, respectively. The electrolyte for both half-cells and full-cells consisted of 1 M $LiPF_6$ and 5% fluoroethylene carbonate (FEC) dissolved in a 1:1:1 (volume ratio) mixture of ethylene carbonate (EC), ethyl methyl carbonate (EMC), and diethyl carbonate (DEC). CR2032 coin cells were assembled in an argon-filled glove box with oxygen and water levels below 0.1 ppm and then used for electrochemical testing. Charge-discharge tests for both half-cells and full-cells were conducted using a Neware test system (BTS-5V10mA) within a voltage range of 0.01-1.5 V.

For the preparation of $LiNi_{0.8}Co_{0.1}Mn_{0.1}O_2$(NCM811) cathodes, the active material, conductive carbon black (Super P), and polyvinylidene fluoride (PVDF) binder were mixed in a mass ratio of 8:1:1 in N-methyl-2-pyrrolidone (NMP) to form a homogeneous slurry. The slurry was coated onto aluminum foil current collectors and dried at 110°C for 12 hours. The N/P ratio was set at 1.1, with a voltage window of 2.7-4.25 V and a current density of 1C (1C = 200 mAg^{-1}). Prior to assembling the full-cells, the M-SiO_x anodes were pretreated for five cycles in half-cells. Electrochemical impedance spectroscopy (EIS)

ISSN 2616-5880 Vol. 6, Issue 1: 59-65, DOI: 10.25236/AJMC.2025.060107

and cyclic voltammetry (CV) tests were performed on a Shanghai Chenhua electrochemical workstation (CHI660E).

3. Results and discussions

3.1 Physicochemical characterization of materials

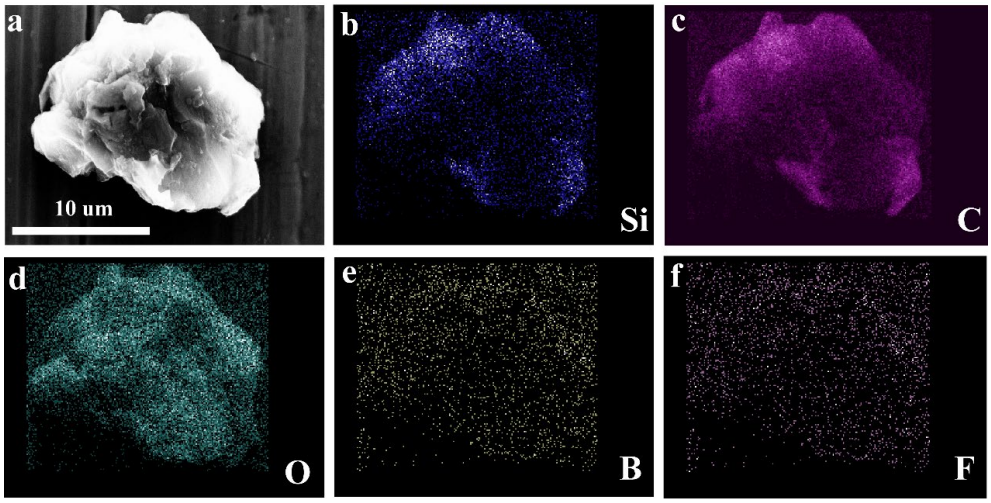

Figure.1. The EDS elemental composition mapping images of M-SiO_x.

SEM and EDS analyses revealed the morphological features and elemental composition of the M-SiO_x sample. As shown in Figure1b-f, the elements F, B, C, and O are uniformly distributed on the surface of the M-SiO_x particles. This finding strongly supports the presence of compounds such as LiF, $Li_2C_2O_4$, $LiBO_2$, and $Li_2B_4O_7$ on the surface of the M-SiO_x sample. As illustrated in Figure 1c, the carbon element originating from the pyrolysis of LiDFOB is clearly observed, and the carbon coating is expected to effectively enhance its electrochemical performance, contributing to improved conductivity of SiO_x, flexibility of the electrode, and stability of the SEI layer.

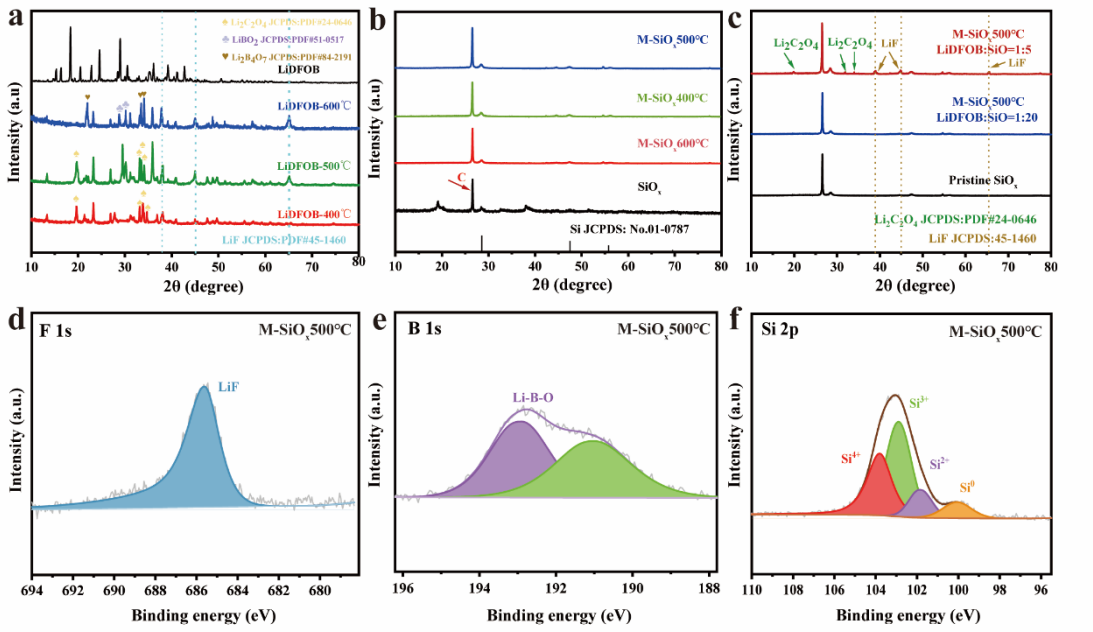

Figure.2. (a) XRD patterns of LiDFOB calcined at different temperatures; (b) XRD patterns of M-SiO_x and SiO_x; (c) XRD patterns of M-SiO_x and SiO_x at different LiDFOB:SiO_x ratios; (d-f) XPS analysis of M-SiO_x composite material calcined at 500°C.

ISSN 2616-5880 Vol. 6, Issue 1: 59-65, DOI: 10.25236/AJMC.2025.060107

As depicted in Figure 2a, during the progressive thermal breakdown of pure LiDFOB salt in an inert environment, the XRD patterns successively reveal characteristic peaks corresponding to compounds like LiF, $Li_2C_2O_4$, $LiBO_2$, and $Li_2B_4O_7$. According to the findings of Wang[16] and Fan[17], the activation energies for lithium-ion migration in these compounds are 1.091 eV (LiF), 0.761 eV ($Li_2C_2O_4$), 0.973 eV ($LiBO_2$), and 0.942 eV ($Li_2B_4O_7$), respectively. Given the relatively weak ionic conductivity of LiF, $Li_2C_2O_4$, $LiBO_2$, and $Li_2B_4O_7$, with their lower activation energies, can effectively accelerate Li^+ migration, thereby compensating for this deficiency.Therefore, through the thermal breakdown of LiDFOB salt, we can form in advance a carbon-containing protective layer on the SiO_x surface that is mechanically stable and enhances rapid Li^+ conduction, while also achieving prelithiation.

By ball-milling and subsequently calcining a small amount of LiDFOB salt with SiO_x, a robust and highly conductive artificial protective layer (modified SiO_x, abbreviated as M-SiO_x500℃, where 500 °C represents the optimal calcination temperature based on specific capacity and cycling stability considerations) is formed on the surface of SiO_x particles. Figure 2c presents the XRD patterns of modified samples M-SiO_x with different mass ratios (LiDFOB:SiO_x = 1:20 and 1:5) and unmodified SiO_x. As shown in Figure 2b, the diffraction peaks at 28.4°, 47.0°, and 55.8° in all samples correspond to crystalline silicon (JCPDS No. 01-0787).In Figure 2c, when comparing M-SiO_x (LiDFOB:SiOx = 1:5) to pristine SiO_x, the extra diffraction peaks located at 38.7°, 44.9°, and 65.5° are ascribed to crystalline LiF, whereas the peaks found at 19.8°, 32.3°, and 33.9° correspond to crystalline $Li_2C_2O_4$. Nevertheless, owing to the reduced concentration of LiF and $Li_2C_2O_4$ in M-SiO_x (LiDFOB:SiO_x=1:20), the corresponding diffraction peaks are not discernible in its XRD pattern.

Subsequently, X-ray photoelectron spectroscopy (XPS) analysis further reveals the chemical composition of the M-SiO_x surface. In the F 1s XPS spectrum, the peak at 685.8 eV is attributed to the formation of LiF (Figure 2d). The B 1s XPS spectrum indicates the presence of Li-B-O in M-SiO_x (Figure 2e). This suggests that the calcination process associated with the thermal decomposition of LiDFOB is actually a thermally driven prelithiation process, which helps to enhance the initial Coulombic efficiency (ICE) of SiO_x. Furthermore, the Si 2p XPS spectrum is deconvoluted based on the different valence states of Si (Figure 4h). As shown in Figure 2f, compared to SiO_x, the content of Si^{4+} decreases and that of Si^0 increases in M-SiO_x, with the average Si valence state dropping from 3.23 to 2.89. This reduction in silicon valence state may be related to the role of graphitic carbon as a reductant during the pyrolysis process, indicating that M-SiO_x will have a higher specific capacity.

In summary, through the pyrolysis of LiDFOB, we have successfully pre-constructed a mechanically stable and rapid Li^+-conducting protective layer composed of LiF, $Li_2C_2O_4$, $LiBO_2$, and $Li_2B_4O_7$ on the SiO_x surface.This interface chemical modulation strategy is expected to significantly enhance the specific capacity, ICE, and cycling stability of silicon monoxide anodes.

3.2 Electrochemical Characterization of Materials

Cyclic voltammetry (CV) tests were conducted on SiO_x and M-SiO_x anodes within a voltage range of 0.01 to 1.5 V (vs Li/Li^+) at a scan rate of 0.1 mV/s. The results are presented in Figures 3a-b. In Figures 3a-b, the reduction peak at 0.05 V for the SiO_x anode corresponds to the formation of Li_xSi, while the cathodic peak near 0.17 V is attributed to the formation of the solid electrolyte interface (SEI). The two oxidation peaks at 0.27 V and 0.53 V are associated with the delithiation process. As cycling progresses, the peaks formed by the lithiation/delithiation reactions become sharper, indicating the progressive nature of this reaction. Compared to the CV curve of the SiO_x anode, the CV curve of the M-SiO_x (treated at 500°C) anode exhibits higher overlap, suggesting a more stable SEI for the M-SiO_x500°C anode. Furthermore, the peaks of the M-SiO_x500°C anode are higher than those of the SiO_x anode, indicating lower internal resistance. Its highly conductive structure facilitates rapid transport of lithium ions and electrons from the electrolyte/electrode interface to the internal silicon particles. Subsequently, we evaluated the SiO_x anode and the modified SiO_x anode in a half-cell configuration to verify the superiority of the modified anode over the pristine SiO_x. As shown in Figure 3c, at a current density of 0.1 Ag^{-1}, the M-SiO_x500°C anode exhibits an initial reversible specific capacity of up to 988.0 $mAhg^{-1}$, significantly higher than the 502.3 $mAhg^{-1}$ of the SiO_x anode. M-SiO_x500°C exhibits a higher reversible capacity, due to its lower mean Si valence state. Furthermore, the lithiation plateau of M-SiO_x500°C is both lower and extended, a feature that corresponds to silicon's lithiation behavior, indicating a relatively higher proportion of Si^0 in M-SiO_x500°C.

In Figure 3d, it can be observed that the ICE of the M-SiO_x (500°C) electrode is 82.0 % in the first cycle, compared to only 72.9 % for the SiO_x electrode. Examining the first discharge curve of the M-SiO_x anode, we find that the reductive decomposition of the electrolyte associated with SEI layer

ISSN 2616-5880 Vol. 6, Issue 1: 59-65, DOI: 10.25236/AJMC.2025.060107

formation is significantly suppressed in the voltage range of 1.0 to 0.25 V. This indicates that the pre-constructed artificial protective layer can effectively mitigate electrolyte decomposition, thereby enhancing ICE and reducing the loss of active lithium. Given the significant impact of rate performance on output power, we tested the cycling performance at different current densities (Figure 3e). Clearly, the M-SiO_x electrode exhibits higher discharge capacities and more stable capacity retention rates at various current densities compared to SiO_x. This excellent performance is attributed to the pre-constructed protective layer on the M-SiO_x surface, composed of LiF, $Li_2C_2O_4$, $LiBO_2$, and $Li_2B_4O_7$, which is not only mechanically robust but also facilitates rapid Li^+ transport, enhancing the interfacial kinetics of charge carriers (lithium ions/electrons) and effectively improving discharge capacity and the reversibility of electrochemical reactions. Furthermore, we tested the cycling stability and corresponding Coulombic efficiency of the samples at current densities of $0.5Ag^{-1}$. As shown in Figures 3g-h, at a current density of $0.5Ag^{-1}$, the reversible specific capacity of the M-SiO_x500°C electrode remains as high as 476.2 $mAhg^{-1}$ after 200 cycles, demonstrating excellent cycling stability.

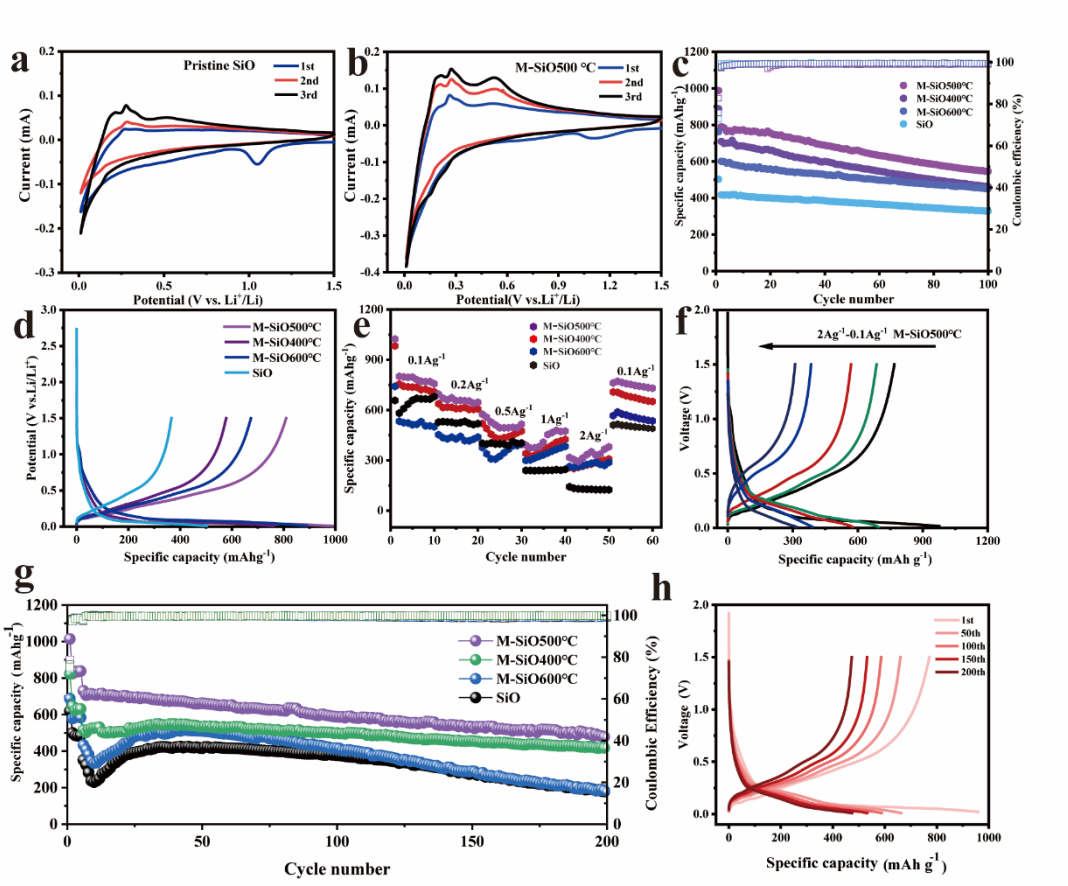

Figure.3. (a) CV curve of SiO_x at 0.1 mVs^{-1}; (b) CV curve of M-SiO_x at 0.1 mVs^{-1}; (c) Long-cycle performance of four electrode materials at $0.1Ag^{-1}$; (d) Charge-discharge curves of four electrode materials at a current density of $0.1Ag^{-1}$; (e) Rate performance of four electrodes; (f) Charge-discharge curves of M-SiO_x at different current densities; (g) Long-cycle performance of four electrodes at $0.5Ag^{-1}$; (h) Charge-discharge curve of M-SiO_x500°C electrode at $0.5Ag^{-1}$.

To delve into the potential of M-SiO_x anode material in practical applications, we assembled and tested an NCM811‖M-SiO_x full-cell system (with a voltage range set at 2.7-4.25 V and an N/P ratio of 1.1). The full-cell underwent 5 activation cycles at a current rate of 0.1 C, followed by subsequent cycling tests at 0.5 C (the specific results are shown in Figure 4b). Upon completion of 200 cycles, the capacity retention of the entire cell remained consistent at 89.7%, decreasing from an initial capacity of 160.4 $mAhg^{-1}$ to 143.9 $mAhg^{-1}$, while exhibiting an average Coulombic efficiency (ICE) as high as 99.6%. Notably, the gradual capacity fade observed in the NCM811‖SiO_x battery is largely attributed to the degradation of bulk electrode materials and the failure of the electrode/electrolyte interfacial layer. It is worth emphasizing that despite not specifically optimizing the binder or electrolyte in this study, significant improvements in cycle life were achieved for both half-cells and full-cells.

ISSN 2616-5880 Vol. 6, Issue 1: 59-65, DOI: 10.25236/AJMC.2025.060107

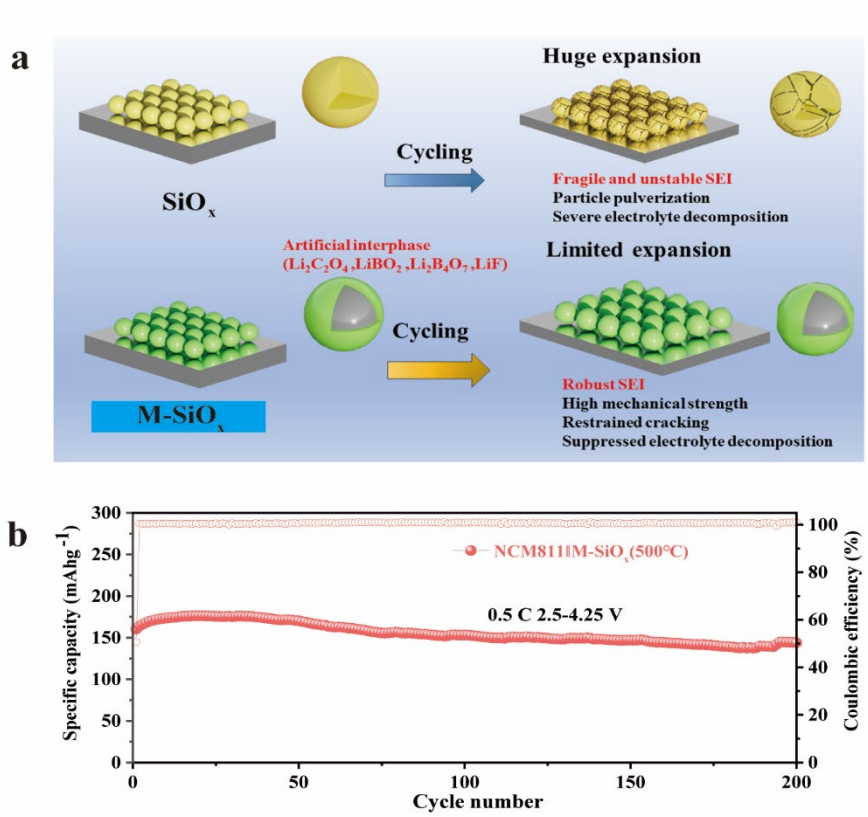

Figure.4. (a) Diagrammatic depiction of the working principle of the pre-fabricated robust and swift ion-conducting layer on the SiOx anode; (b) Long-term cycling performance of the NCM811||M-SiO_x full cell at 0.5 C;

4. Conclusion

In summary (as illustrated in Figure 4a), we ingeniously utilized the pyrolysis process of LiDFOB salt to meticulously construct a robust and durable fast ion-conducting interfacial artificial protective layer on the surface of SiO_x particles. This artificial protective layer not only endowed the SEI layer with excellent mechanical strength but also ensured efficient conduction of Li^+ ions. Consequently, it effectively accommodated the plastic deformation and microcracks generated during the charge-discharge process of the SiO_x anode, significantly suppressed parasitic reactions, and maintained the integrity of the electrode structure throughout cycling. Thanks to this, the M-SiO_x electrode exhibited a higher initial Coulombic efficiency (ICE), superior capacity retention, and enhanced rate performance compared to the untreated SiO_x electrode. Notably, when the M-SiO_x anode was paired with an NCM811 cathode to form a full-cell, the battery maintained a high capacity retention of 89.7% after 200 cycles. This study profoundly reveals the crucial role of pre-constructing an artificial SEI layer and modulating interfacial chemical properties in enhancing the overall performance of silicon monoxide-based anodes.

References

[1] Xu S, Hou X, Wang D, et al. Insights into the Effect of Heat Treatment and Carbon Coating on the Electrochemical Behaviors of SiO Anodes for Li-Ion Batteries[J]. Advanced Energy Materials, 2022, 12(18): 2200127.

[2] Bian C, Fu R, Shi Z, et al. Mg_2SiO_4/Si-coated disproportionated SiO composite anodes with high initial coulombic efficiency for lithium ion batteries[J]. ACS Applied Materials & Interfaces, 2022, 14(13): 15337-15345.

[3] Zhang Y, Guo G, Chen C, et al. An affordable manufacturing method to boost the initial Coulombic efficiency of disproportionated SiO lithium-ion battery anodes[J]. Journal of Power Sources, 2019, 426: 116-123.

[4] Han J, Jo S, Na I, et al. Homogenizing silicon domains in SiO_x anode during cycling and enhancing

ISSN 2616-5880 Vol. 6, Issue 1: 59-65, DOI: 10.25236/AJMC.2025.060107

battery performance via magnesium doping[J]. ACS Applied Materials & Interfaces, 2021, 13(44): 52202-52214.
[5] Tan Y, Jiang T, Chen G Z. Mechanisms and product options of magnesiothermic reduction of silica to silicon for lithium-ion battery applications[J]. Frontiers in Energy Research, 2021, 9: 651386.
[6] Raza A, Jung J Y, Lee C H, et al. Swelling-Controlled Double-Layered SiO_x/Mg_2SiO_4/SiO_x Composite with Enhanced Initial Coulombic Efficiency for Lithium-Ion Battery[J]. ACS applied materials & interfaces, 2021, 13(6): 7161-7170.
[7] Shi L, Pang C, Chen S, et al. Vertical graphene growth on SiO microparticles for stable lithium ion battery anodes[J]. Nano Letters, 2017, 17(6): 3681-3687.
[8] Tian Y F, Li G, Xu D X, et al. Micrometer-Sized $SiMg_yO_x$ with Stable Internal Structure Evolution for High-Performance Li-Ion Battery Anodes[J]. Advanced Materials, 2022, 34(15): 2200672.
[9] Zhang Y, Jiang Y, Li Y, et al. Preparation of nanographite sheets supported Si nanoparticles by in situ reduction of fumed SiO_2 with magnesium for lithium ion battery[J]. Journal of Power Sources, 2015, 281: 425-431.
[10] Li Z, Zhao H, Wang J, et al. Rational structure design to realize high-performance SiO_x@C anode material for lithium ion batteries[J]. Nano Research, 2020, 13: 527-532.
[11] Goodenough J B, Park K S. The Li-ion rechargeable battery: a perspective[J]. Journal of the American Chemical Society, 2013, 135(4): 1167-1176.
[12] Xu G, Shangguan X, Dong S, et al. Formulation of blended-lithium-salt electrolytes for lithium batteries[J]. Angewandte Chemie International Edition, 2020, 59(9): 3400-3415.
[13] Fan X, Wang C. High-voltage liquid electrolytes for Li batteries: progress and perspectives[J]. Chemical Society Reviews, 2021, 50(18): 10486-10566.
[14] Min X, Han C, Zhang S, et al. Highly Oxidative-Resistant Cyano-Functionalized Lithium Borate Salt for Enhanced Cycling Performance of Practical Lithium-Ion Batteries[J]. Angewandte Chemie International Edition, 2023, 62(34): e202302664.
[15] Ren Z, Qiu H, Fan C, et al. Delicately Designed Cyano-Siloxane as Multifunctional Additive Enabling High Voltage $LiNi_{0.9}Co_{0.05}Mn_{0.05}O_2$/Graphite Full Cell with Long Cycle Life at 50 °C[J]. Advanced Functional Materials, 2023, 33(36): 2302411.
[16] Wang X, Xiao R, Li H, et al. Oxygen-driven transition from two-dimensional to three-dimensional transport behaviour in β-Li_3PS_4 electrolyte[J]. Physical Chemistry Chemical Physics, 2016, 18(31): 21269-21277.
[17] Fan X, Wang C. High-voltage liquid electrolytes for Li batteries: progress and perspectives[J]. Chemical Society Reviews, 2021, 50(18): 10486-10566.